1997

Improvement of estuarine and coastal modeling using high-order difference schemes

Fan, Chenwu; Chu, Peter C.

Chu, P.C., and C.W. Fan, 1997: Improvement of estuarine and coastal modeling using high-order difference schemes. Estuarine and Coastal Modeling, 5, American Society of Civil Engineering, 28-34
http://hdl.handle.net/10945/36268

Improvement of Estuarine and Coastal Modeling Using High-Order Difference Schemes

Peter C. Chu, and Chenwu Fan

Department of Oceanography, Naval Postgraduate School, Monterey, California

Abstract.

How to reduce the computational error is a key issue of using σ-coordinate coastal ocean models. Due to the fact that the higher the order of the difference scheme, the less the truncation error and the more complicated the computation, we introduce three sixth-order difference schemes (ordinary, compact, and combined compact) for the σ-coordinate coastal models in order to reduce error without increasing much complexity of the computation. After the analytical error estimation, the Semi-Spectral Primitive Equation Model (SPEM) is used to demonstrate the benefit of using these schemes and to compare the difference among the three six-order schemes. Over a wide range of parameter space as well as a great parametric domain of numerical stability, the ordinary sixth-order scheme is shown to have error reductions by factors of 50 comparing to the second-order difference scheme. Among the sixth-order schemes, the compact scheme reduces error by more than 50-55% comparing to the ordinary scheme, and the combined compact scheme reduces error by more than 60% comparing to the compact scheme.

1. Introduction

Most estuarine and coastal models use second-order difference schemes (such as second-order staggered C-grid scheme) to approximate first-order derivative (Blumberg and Mellor, 1987; Hadivogel et al., 1991)

$$\left(\frac{\partial p}{\partial x}\right)_i \simeq \frac{p_{i+1/2} - p_{i-1/2}}{\Delta} - \frac{1}{24}\left(\frac{\partial^3 p}{\partial x^3}\right)_i \Delta^2, \quad (1)$$

where p, Δ represent pressure and grid spacing. Such a difference scheme was proposed by numerical modelers in early 50's as the first generation computers came into place. Since then the computer updates rapidly with several orders of magnitude increase in computational power. However, the difference schemes used by most modelers now are still staying at the 50's level (second-order schemes).

Besides, the current scheme uses the local Lagrangian Polynomials whose derivatives are discontinuous. Figure 1 shows the process of computing first-order derivative of function $\phi(x)$ at five neighboring grid points. At the grid x_i, $\phi'(x_i)$ is the tangential of the Lagrangian Polynomial L_i at x_i. As i increases, three neighboring L_{i-1}, L_i, L_{i+1} have different tangential at the point x_i. Such a hidden problem in discretization might distort the physical processes.

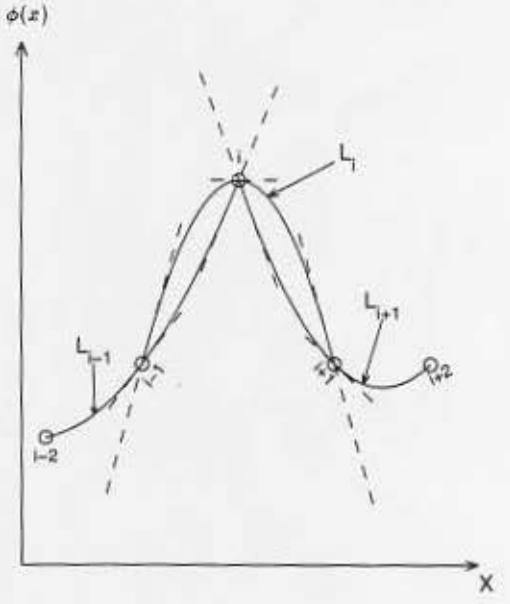

Figure 1. Discontinuity of the first derivatives of the Lagrangian Polynomials at each grid point.

2. Six-Order Ordinary Difference (OD) Scheme

Since the truncation error decreases with the increase of the order of the difference scheme, it might be benefited to use a higher order difference schemes. For example, Chu and Fan [1997a] proposed to use a six-order ordinary difference scheme

$$\left(\frac{\partial p}{\partial x}\right)_i \simeq \left(\frac{-9p_{i-5/2}+125p_{i-3/2}-2,250p_{i-1/2}}{1920\Delta}\right) + \left(\frac{2,250p_{i+1/2}-125p_{i+3/2}+9p_{i+5/2}}{1920\Delta}\right) - \frac{5}{7,168}\left(\frac{\partial^7 p}{\partial x^7}\right)_i \Delta^6, \quad (2)$$

to compute the horizontal pressure gradient. Comparing (2) with (1), the error ratio between the sixth-order and second-order schemes is estimated by

$$r_{6,2} = \left|\frac{\frac{5}{7168}\left(\frac{\partial^7 p}{\partial x^7}\right)_i}{\frac{1}{24}\left(\frac{\partial^3 p}{\partial x^3}\right)_i}\right| \Delta^4 = 0.0167\left|\frac{\left(\frac{\partial^7 p}{\partial x^7}\right)_i}{\left(\frac{\partial^3 p}{\partial x^3}\right)_i}\right| \Delta^4. \quad (3)$$

which is proportional to Δ^4.

There are two weaknesses of using ordinary high-order difference schemes. The first one is more grid points (6 points) needed for the computation. The second one is using lower-order schemes at two boundaries.

3. Sixth-Order Compact Difference (CD) Scheme

The compact scheme is used to overcome such a weakness by connecting the derivative at the grid with that at the two neighboring grids, e.g.,

$$\alpha^+\left(\frac{\partial p}{\partial x}\right)_{i+1} + \alpha^0\left(\frac{\partial p}{\partial x}\right)_i + \alpha^-\left(\frac{\partial p}{\partial x}\right)_{i-1} = \beta_1 p_{i+3/2} + \beta_2 p_{i+1/2} + \beta_3 p_{i-1/2} + \beta_4 p_{i-3/2}. \quad (4)$$

The parameters $\alpha^0, \alpha^+, \alpha^-, \beta_1, \beta_2, \beta_3, \beta_4$ are determined by requiring the minimum error (Chang and Shirer, 1985). Such compact schemes guarantee continuity of the first derivative at each grid point.

By requiring the minimum truncation error for the sixth-order difference scheme we obtain the sixth-order compact scheme (Chu and Fan, 1997b)

$$\frac{1}{80}\left[9\left(\frac{\partial p}{\partial x}\right)_{i-1} + 62\left(\frac{\partial p}{\partial x}\right)_i + 9\left(\frac{\partial p}{\partial x}\right)_{i+1}\right] = \frac{1}{240}\frac{-17p_{i-3/2}-189p_{i-1/2}+189p_{i+1/2}+17p_{i+3/2}}{\Delta} - \frac{117}{358,400}\left(\frac{\partial^7 p}{\partial x^7}\right)_i \Delta^6, \quad (5a)$$

The "left" boundary point is computed by

$$\left(\frac{\partial p}{\partial x}\right)_1 = \frac{1,627}{1,920}p_{1/2} - \frac{211}{640}p_{3/2} - \frac{59}{48}p_{5/2} + \frac{235}{192}p_{7/2} - \frac{91}{128}p_{9/2} + \frac{443}{1,920}p_{11/2} - \frac{31}{960}p_{13/2} + \frac{3,043}{107,520}\left(\frac{\partial^7 p}{\partial x^7}\right)_i \Delta^6 \quad (5b)$$

The "right" boundary point has the similar formulation. The last terms in (2) and (5) suggest that the compact scheme can provide more accuracy. The error ratio between the sixth-order compact and ordinary schemes is

$$r_6 = \frac{\left|-\frac{117}{358,400}\left(\frac{\partial^7 p}{\partial x^7}\right)_i \Delta^6\right|}{\left|\frac{5}{7,168}\left(\frac{\partial^7 p}{\partial x^7}\right)_i \Delta^6\right|} = 46.8 \quad (6)$$

which means a more than 50% reduction of the truncation error when we use the compact scheme for the 6th-order accuracy. We use the pressure gradient error reduction in the σ-coordinate system as an example to illustrate the benefit of using high-order compact difference schemes.

4. Sixth-Order Combined Compact Difference (CCD) Scheme

Recently, Chu and Fan (1998) proposed a three-point combined compact scheme

$$\left(\frac{\delta p}{\delta x}\right)_i + \alpha_1\left(\left(\frac{\delta p}{\delta x}\right)_{i+1} + \left(\frac{\delta p}{\delta x}\right)_{i-1}\right) + \beta_1\Delta\left(\left(\frac{\delta^2 p}{\delta x^2}\right)_{i+1} - \left(\frac{\delta^2 p}{\delta x^2}\right)_{i-1}\right) + \ldots = \frac{a_1}{2\Delta}(f_{i+1} - f_{i-1}) \quad (7)$$

$$\left(\frac{\delta^2 p}{\delta x^2}\right)_i + \alpha_2\left(\left(\frac{\delta^2 p}{\delta x^2}\right)_{i+1} + \left(\frac{\delta^2 p}{\delta x^2}\right)_{i-1}\right) + \beta_2\frac{1}{2\Delta}\left(\left(\frac{\delta p}{\delta x}\right)_{i+1} - \left(\frac{\delta p}{\delta x}\right)_{i-1}\right) + \ldots = \frac{a_2}{\Delta^2}(f_{i+1} - 2f_i + f_{i-1}) \quad (8)$$

to compute p_i' , p_i'',...$p_i^{(k)}$ by means of the values and derivatives at the two neighboring points. Moving from the one boundary to the other, CCD forms a global algorithm to compute various derivatives at all grid points, and guarantees continuity of all derivatives at each grid point.

5. Pressure Gradient Error in the σ-Coordinate System

Coastal ocean models usually use a terrain-following σ-coordinate system to handle the effects of bottom topography. Here the water column is divided into the same number of grid cells independence of depth . Let (x_*, y_*, z) denote Cartesian coordinates and (x, y, σ) sigma coordinates. In most sigma coordinate ocean models the relationship between the two coordinate systems are:

$$x = x_*, \qquad y = y_*, \qquad \sigma = 1 + 2\frac{z}{H(x,y)} \tag{9}$$

where z and σ increase vertically upward such that $z = 0, \sigma = 1$ at the surface and $z = -H$ and $\sigma = -1$ at the bottom. $H = H(x, y)$ is the bottom topography.

A problem has long been recognized in computing the horizontal pressure gradient in the σ-coordinate system (e.g., Gary, 1973; Haney, 1991; and Mellor et al., 1994, McCalpin, 1994): the horizontal pressure gradient becomes a difference between two terms, which leads to a large truncation error at a steep topography.

6. Seamount Test Case

6.1 Model Description

Suppose a seamount located inside a periodic f-plane ($f_0 = 10^{-4}\mathrm{s}^{-1}$) channel with two solid, free-slip boundaries along constant y. Unforced flow over seamount in the presence of resting, level isopycnals is an idea test case for the assessment of pressure gradient errors in simulating stratified flow over topography. The flow is assumed to be reentrant (periodic) in the along channel coordinate (i.e., x-axis). We use this seamount case of the Semi-spectral Primitive Equation Model (SPEM) version 3.9 to test the new difference scheme. The reader is referred to the original reference (Haidvogel et al., 1991) and the SPEM 3.9 User's Manuel (Hedstrom, 1995) for detail information. In the horizontal directions the model uses the C-grid and the second-order finite difference discretization except for the horizontal pressure gradient, which the user has choice of either second-order or fourth-order difference discretization (McCalpin, 1994). In the vertical direction the model uses a boundary fitted σ-coordinate system. The discretization is by spectral collocation using Chebyshev polynomials. Our model configuration is similar to that of Beckmann and Haidvogel (1993), McCalpin (1994), and Chu and Fan (1997a). The time step and grid size used here are,

$$\Delta t = 675s, \Delta x = \Delta y = 5km. \tag{10}$$

6.2 Topography

The domain is a periodic channel, 320 km long and 320 km wide. The channel walls are solid (no normal flow) with free-slip viscous boundary conditions. The channel has a far-field depth h_{max} and in the center includes an isolated Gaussian-shape seamount with a width L and an amplitude h_s(Figure 2),

$$h(x,y) = h_{\max} - h_s \exp\left[-\frac{(x-x_0)^2 + (y-y_0)^2}{L^2}\right] \tag{11}$$

where (x_0, y_0) are the longitude and latitude of the seamount center. The far-field depth (h_{max}) is fixed as 5,000 m. But the seamount amplitude (h_s) changes from 500 to 4,500 m, and the lateral scale of the seamount (L) varies from 10 to 40 km. for the study.

6.3 Density Field

The fluid is exponentially stratified and initially at rest. The initial density field has the form,

$$\rho_i = \overline{\rho}(z) + \widehat{\rho}\exp(\frac{z}{H_\rho}) \tag{12}$$

where z is the vertical coordinate, and $H_\rho = 1000$ m, and

$$\overline{\rho}(z) = 28 - 2.\exp(\frac{z}{H_\rho}) \tag{13}$$

is a reference density field. Here a constant density, 1000 kg m^{-3}, has been subtracted for the error reduction. Following Beckmann and Haidvogel (1993) and McCalpin (1994), we subtract the mean density field $\overline{\rho}(z)$ before integrating the density field to obtain pressure from the hydrostatic equation.

The density anomaly, $\widehat{\rho}$, indicates that the initial condition of the model was slightly less stably stratified than the reference field for each computation. In this study, the density anomaly varies from 0.1-1 kg m^{-3}.

6.4 Lateral Viscosity

Ideally, the new difference scheme should be tested with no lateral diffusion of density. This is due to the fact that the density diffusion along σ surfaces generates horizontal gradients wherever the σ surfaces are not flat, and then produces horizontal pressure gradients which drive currents in much the same way as the pressure gradient errors (McCalpin, 1994). Unfortunately, the absence of the horizontal diffusion keeps the small-scale pressure disturbances generated by topographic scale density advection, and the induced small-scale velocity fields, which in turn cause the computational instability problem. Thus, some lateral viscosity on σ surfaces is required in the momentum equations to maintain stability. A constant coefficient (A_H) biharmonic formulation is used here for the lateral viscosity, which varies from $10^{10} - 10^{8}$ $m^4 s^{-1}$ in this study.

7. Standard Case

7.1 Model Parameters

At first, we set up a standard test case to compare errors among the ordinary, compact, and combined compact difference schemes: L = 40 km, h_s = 4,500 m,

$$\widehat{\rho} = 0.2 kg m^{-3}, \; A_H = 10^{10} m^4 s^{-1} \qquad (14)$$

Figure 3 displays results from the sixth-order compact case: the error in the streamfunction and velocity fields after performing 5 days of integration. The mass transport streamfunction has a large-scale eight-lobe pattern centered on the seamount. This symmetric structure can be found in all the fields. After 5 days of integration, the model generates spurious currents of O(0.03 cm/s), much smaller than that of O(6 cm/s) generated with the second order scheme and O(0.2 cm/s) generated with the fourth order ordinary scheme (Figures 1 and 2 in McCalpin, 1994).

7.2 Temporal Variations of Peak Error Velocity

Owing to a very large number of calculations performed, we discuss the results exclusively in terms of the maximum absolute value the spurious velocity (called peak error velocity) generated by the pressure gradient errors. Figure 4 shows the time evolution of the peak error velocity for the first 20 days of integration with the second-, fourth-, and sixth-order ordinary schemes. Figure 5 shows the time evolution of the peak error velocity with the sixth-order ordinary, compact, and combined compact schemes. The peak error velocity fluctuates rapidly during the first few days integration. After the 5 days of integration, the peak error velocity show the decaying inertial oscillation superimposed into asymptotic values. The asymptotic value is near 10^{-4} m/s for the ordinary scheme, 0.44×10^{-4} m/s for the compact scheme, and 0.16×10^{-4} m/s for the combined compact scheme. Thus, the compact scheme reduces error by more than 50-55% comparing to the ordinary scheme, and the combined compact scheme reduces error by more than 60% comparing to the compact scheme.

8. Conclusions

(1) The σ-coordinate, pressure gradient error depends on the choice of difference schemes. By choosing an optimal scheme, we may reduce the error in a great deal without increasing the horizontal resolution. Analytical analysis shows that the truncation error ratio between the fourth-order scheme and the second-order scheme is proportional to Δ^2, and the truncation error ratio between the sixth-order scheme and the second-order scheme is proportional to Δ^4. The compact scheme may reduce near 30% error for the fourth-order difference and more than 50% error for the sixth order difference.

(2) The SPEM Version 3.9 is used to demonstrate the benefit of using the sixth-order scheme. A series of calculations of unforced flow in the vicinity of an isolated seamount are performed. Over a wide range of parameter space as well as a great parametric domain of numerical stability, the sixth-order scheme has error reductions by factors of 50 comparing to the second-order difference scheme. Furthermore, the compact scheme reduces error by more than 50-55% for the sixth-order difference scheme, and the combined compact scheme reduces error by more than 60% comparing to the compact scheme.

(3) Using the sixth-order scheme does not require much more CPU time. Taking SPEM3.9 as an example, the CPU time for the sixth-order scheme is almost the same as for the fourth-order scheme, and 10% more than for the second-order scheme, and the CPU time for the compact scheme (both fourth- and sixth-order) is only 5% more than the ordinary scheme.

(4) Since the fourth-order different scheme has error reductions by factors of 10 comparing to the second-order difference scheme, there is no real advantage to going to a higher order scheme if the bottom topography is not too complicated. The need for a lot of accuracy will go up with increasingly complex bottom topography on small scales, so one might expect that future demand of the accuracy will increase as models strive for more realism.

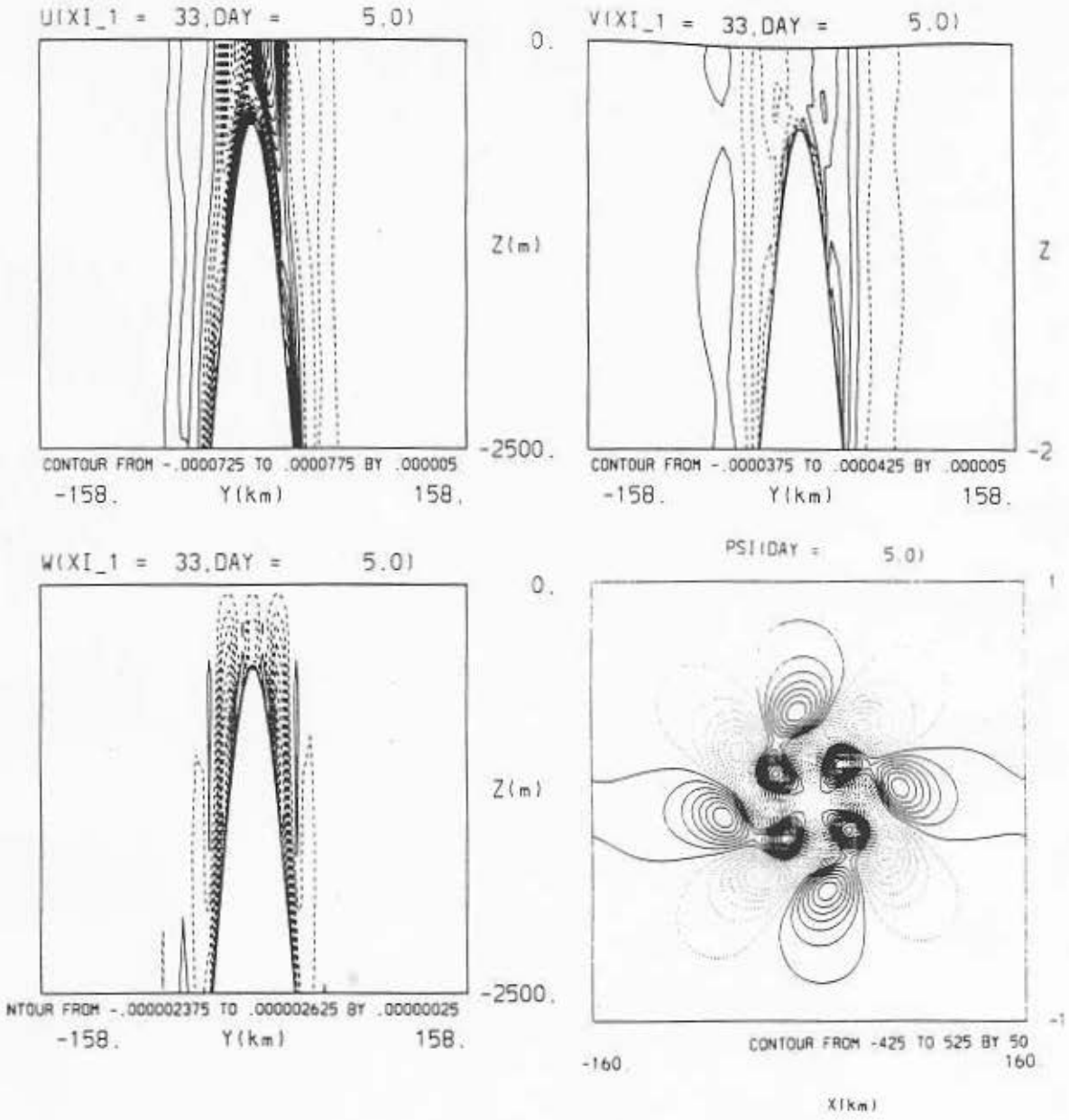

Figure 3. Instantaneous error pattern after 5 days of integration for the unforced experiment with sixth-order compact scheme: (a) u, (b) v, (c) w, and (d) mass transport streamfunction. Here u, v, w are evaluated at the slice (facing upchannel) through the center of the seamount (after Chu and Fan, 1997a.)

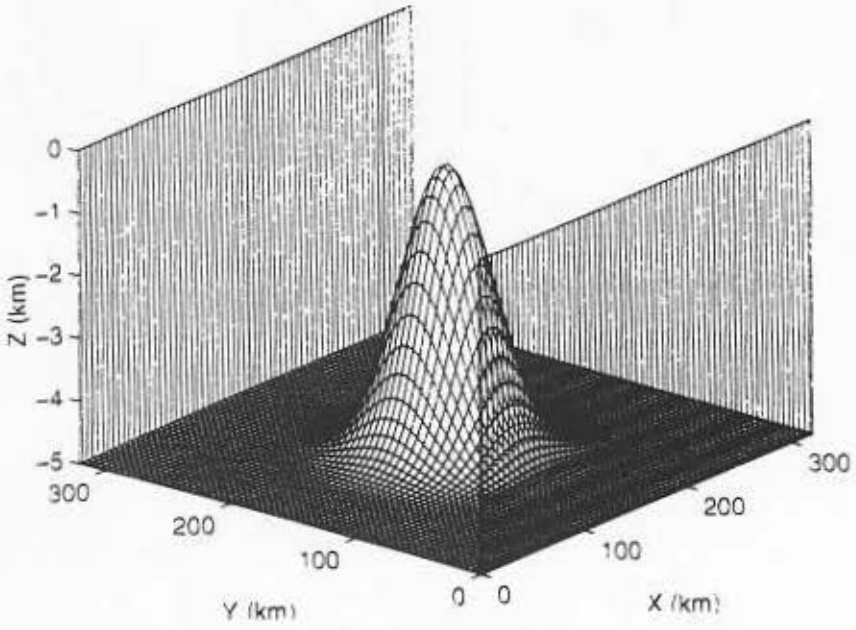

Figure 2. The seamount geometry.

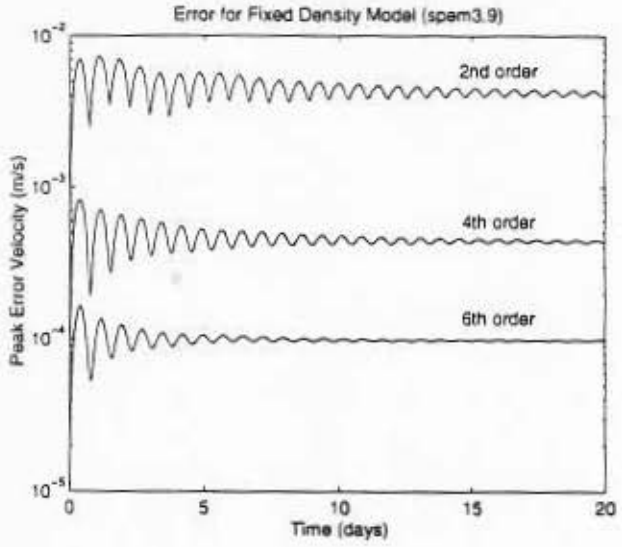

Figure 4. Peak error velocity for the second-, fourth-, and sixth-order ordinadry schemes (after Chu and Fan, 1997a.)

Acknowledgments

The authors wish to thank Dale Haidvogel and Kate Hedstrom of the Rutgers University for most kindly proving us with a copy of the SPEM code. This work was funded by the Office of Naval Research NOMP Program, the Naval Oceanographic Office, and the Naval Postgraduate School.

References

Beckmann, A., and D. B. Haidvogel, 1993: Numerical simulation of flow around a tall isolated seamount. Part 1: Problem formulation and model accuracy. *J. Phys. Oceanogr.*, **23**, 1736-1753.

Chang, H.R., and H.N. Shirer, 1985: Compact spatial differencing techniques in numerical modeling. *Mon. Wea. Rev.*, **113**, 409-423.

Chu, P.C., and C.W. Fan, 1997a: A sixth-order difference scheme in sigma coordinate ocean models. *J. Phys. Oceanogr.*, **27**, 2064-2071.

Chu, P.C., and C.W. Fan, 1997b: Compact difference schemes sigma coordinate ocean models. *Internat. J. Num. Methods in Fluids*, submitted.

Chu, P.C., and C.W. Fan, 1998: A three-point combined compact difference scheme. *J. Compt. Phys.*, **140**, 1-30.

Gary, J.M., 1973: Estimate of truncation error in transformed coordinate primitive equation atmospheric models, *J. Atmos. Sci.*, **30**, 223-233.

Haidvogel, D.B., J.L. Wikin, and R. Young, 1991: A semi-spectral primitive equation model using vertical sigma and orthogonal curvilinear coordinates. *J. Comput. Phys.*, **94**, 151-185.

Haney ,1991: On the pressure gradient force over steep topography in sigma coordinate ocean models. *J. Phys. Oceanogr.*, **21**, 610-619.

Hedstrom, K., 1994: User's Manual for a Semi-Spectral Primitive Equation Ocean Circulation Model Version 3.9, Rutgers University, New Jersey.

McCalpin, J.D., 1994: A comparison of second-order and fourth-order pressure gradient algorithms in a σ-coordinate ocean model. *Internat. J. Num. Methods in Fluids*, **18**, 361-383.

Mellor, G.L., T. Ezer, and L.-Y. Oey, 1994: The pressure gradient conundrum of sigma coordinate ocean models. *J. Atmos. Oceanic Technol.*, **11**, 1126-1134.

Sunsqvist, H., 1976: On vertical interpolation and truncation in connection with use of sigma system models. *Atmosphere*, **14**, 37-52.

Robinson, A.R., 1993: Physical precesses, field estimation and interdisciplinary ocean modeling. *Harvard Open Ocean Model Reports***Harvard University**, Cambridge, 71 pp.

P. Chu, and C. Fan, Department of Oceanography, Naval Postgraduate School, Monterey, California. (e-mail: chu@nps.navy.mil)

(Received August 19, 1997; revised February 10, 1998; accepted February 25, 1998.)